UNIVERSITY OF CALIFORNIA SAN DIEGO

Investigating the Accuracy, Precision, and Cooling Rate Dependence of Laboratory-Acquired Thermal Remanences During Paleointensity Experiments

A Thesis submitted in partial satisfaction of the requirements for the degree Master of Science

in

Earth Sciences

by

Christeanne Nicole Santos

Committee in charge:

Lisa Tauxe, Chair
Paterno Castillo
Jane Teranes

2019

The Thesis of Christeanne Nicole Santos is approved, and it is acceptable in quality and form for publication on microfilm and electronically:

Chair

University of California San Diego

2019

DEDICATION

Ito ay para sa aking pamilya.

EPIGRAPH

The arts and sciences are avatars of human creativity.

Mae Jemison

Of course, mankind has made giant steps forward.

However, what we know is really very, very little

compared to what we still have to know.

Fabiola Gianotti

TABLE OF CONTENTS

LIST OF FIGURES

LIST OF TABLES

ACKNOWLEDGMENTS

Another thesis could be written on the gratitude and thanks that I owe to the people who have supported me in this endeavor. Although there is not enough time or paper in the world to fully express this, and at the expense of sounding mildly threatening: you all know who you are, and you all know what you did. Thank you.

I extend very special thanks to Lisa Tauxe: my mentor, my teacher, my mom-visor. Lisa has been such a solid foundation for my accomplishments and for overcoming adversity alike at SIO. I cannot thank her enough for the support, the opportunities, her patience, and for all of the things that I didn't want to hear but I needed.

I also thank my P-Mag family: Hanna Asefaw, Shelby Jones, Sarah Maher, Brendan Cych, Shuhui Cai, Lesleis Nagy, and all others who have come in and out of the lab. I thank them all for the unwavering support, the stimulating conversations, and pressing "cool" for me. I also thank Jeff Gee for his help and giving me my first opportunity to be in the lab.

To my best friends from home: Aaron Tumamao, Monica Cruz, Andrew Perez, Toney Smith, and Gloria Lee; and to my best friends at SIO: L, M, and K (2 4 1), Hanna, and Shelby... the continued unconditional love and support that I have received has been integral to my successes at SIO and outside of campus, and as my growth as a scientist and as a person. Where would I be without you all?

I also extend special thanks to all of the professors, staff, administration, researchers, and support teams of SIO, UCSD, and of the paleomagnetic community. This

work is a community effort, and I am grateful to have all of them and their contributions as such key components of my time spent at SIO and of this thesis. An extra special thanks goes out to my committee members: Paterno Castillo and Jane Teranes, especially for their patience, time, and invaluable advice.

Above all, I thank my family. I am eternally grateful for the unconditional love (soft and tough), support, patience, and for the countless times they have sacrificed something to put me first. This is all for them. A Filipino proverb says: *"Ang hindi lumingon sa pinanggalingan, hindi makakarating sa paroroonan..."* meaning that a person who does not look back at where they come from will never reach their destination.

The abstract and chapter sections of this thesis, in full, are modified versions of a publication as it appears in Geochemistry, Geophysics, Geosystems: Santos, C. N., & Tauxe, L. (2019). Investigating the accuracy, precision, and cooling rate dependence of laboratory-acquired thermal remanences during paleointensity experiments. *Geochem., Geophys., Geosys.*, *20*, 383–397. doi.org/10.1029/2018GC007946. The thesis author is the primary investigator and author of this paper.

ABSTRACT OF THE THESIS

Investigating the Accuracy, Precision, and Cooling Rate Dependence of Laboratory-Acquired Thermal Remanences During Paleointensity Experiments

by

Christeanne Nicole Santos

Master of Science in Earth Sciences

University of California San Diego, 2019

Professor Lisa Tauxe, Chair

Magnetic field intensity is one of Earth's fundamental properties and its temporal behavior has implications in fields ranging from geodynamics to archeology. Thermal remanent magnetization (TRM) has the strongest theoretical basis of all the forms of natural remanent magnetization, and natural and archeological materials have been used to estimate paleointensities for decades. Although founded on sound theory for ideal samples (those that produce linear Arai plots), paleointensity estimation is challenging with non-ideal samples, which are more abundant in nature and widely used in experiments.

We examined the behavior of natural samples using both original and laboratory-acquired TRMs during paleointensity experiments and characterized them based on proxies for domain state including curvature, k, and bulk domain stability parameters. We then investigated their capacity to retain a record of the magnetic field. Samples taken from previous experiments were separated into *straight* and *curved* groups representing single-domain-like from multi-domain-like remanences, respectively, based on a critical threshold value, k = 0.164.

Specimens from the two sets were given a fresh TRM in a 70 μT laboratory field and subjected to an infield-zerofield, zerofield-infield (IZZI)-type paleointensity experiment. *Straight* specimens recovered the laboratory field with high precision while *curved* specimens produced more scattered results. However, both sets closely recovered the average laboratory field, which suggests that experiments containing a sufficient number of specimens can avoid large biases in the field estimate.

We also found that the dependence of cooling rate on the laboratory TRM was significant in most samples. However, it did not depend on their inferred domain states and should be estimated for all samples whose cooling rates differ from the laboratory field. Our results confirm that while ideally behaved specimens can produce accurate and precise paleofield estimates, non-ideal, or *curved*, specimens produce more scattered, although unbiased, estimates.

Chapter 1

Introduction

The strength of the magnetic field is one of the fundamental properties of the Earth and its behavior over time has implications in disparate fields from geodynamics [Biggin et al., 2012] to archaeology [Ben-Yosef et al., 2010]. Of all the forms of remanent magnetization found in nature, thermal remanent magnetization (TRM) has the strongest theoretical basis thanks to the work of Néel [1949] and Thellier [1959], supported by experimental evidence by e.g. Wernsdorfer et al. [1997]. TRM is related to the ambient magnetic field applied during cooling by a hyperbolic tangent function which is quasi-linear for low fields like the Earth's and can be reproduced in the laboratory, making absolute paleointensity estimates possible. Yet, the optimization of techniques for paleointensity determination has been a longstanding debate in the paleomagnetic community [Dunlop, 2011]. The complexities and ambiguities both in the field and in the

laboratory have fostered a multiplicity of approaches to the problem of intensity estimation.

As an example of the complexity of TRM, it has long been suspected that cooling rate may have a strong effect resulting in either an overestimate or an underestimate of the ancient magnetic field [Thellier, 1938]. Despite decades of research, the magnitude and mechanisms controlling the cooling rate dependence of TRM are still subject to debate with some suggesting that remanence dominated by single-domain (SD) particles show a strong cooling rate dependence, while so-called 'pseudo-single-domain' (PSD) and multi-domain (MD) remanences shown no or even a negative cooling rate dependence respectively e.g., [Biggin et al., 2013], [Ferk et al., 2014].

In this thesis we examine the theoretical and experimental constraints on cooling rate from previously published literature in Chapter 2. In Chapter 3 we describe rock magnetic and paleointensity experiments on a sample set selected based on the behavior in published paleointensity experimental data which allow us to separate the samples into 'SD-like', with nearly straight Arai plots [Nagata et al., 1963] of the original paleointensity data and 'non-SD-like' with significantly curved Arai plots using the curvature criterion of Paterson [2011]. In Chapter 4, we present the results of our experiments on fresh laboratory acquired TRMs, and in Chapter 5 we discuss implications for the accuracy and precision of paleointensity estimates of the SD-like (*straight*) specimens versus the non-SD-like (curved) category and compare cooling rate dependence of the remanence with various domain state proxies. Finally, our conclusions are summarized in Chapter 6.

Chapter 2

Background for Cooling Rate Dependence

Starting with Néel [1949], many authors have predicted that the magnetization acquired by a sample will depend on the rate at which it cools. This phenomenon results from the dependence of blocking temperature on cooling rate. Blocking temperature (T_b) is the temperature at which a population of magnetic grains goes abruptly from maintaining equilibrium with an external field to being 'blocked' and unable to maintain equilibrium during cooling at a given rate. T_b depends on relaxation time, τ , which is the time (in seconds) required for the magnetization of a given grain size (and shape) population to decay to $1/e$ of its original magnetization when placed in zero field (e.g. [Tauxe et al., 2010] for a review); therefore τ is strongly dependent on temperature, so T_b

is inherently rate dependent. Because the relaxation time of a given grain increases with decreasing temperature, Néel theory for single-domain magnetizations predicts that the more slowly a sample cools, the longer equilibrium magnetization can be maintained and the stronger the net magnetization will be. The problem with this simple theory from a practical standpoint of, say, correcting for cooling rate dependence from first principles is that such a correction requires integration of non-linear differential equations that are based on a number of poorly constrained assumptions including for example, that the grains are uniaxial, non-interacting, and single-domain, assumptions rarely met in natural materials. Different approaches to the cooling rate problem have led to different predictions regarding the dependence of magnetization and cooling rate as outlined in the following.

2.1 Single-Domain Remanances

Drawing on the theory of Néel, Stacey [1963] predicted a dependence of blocking temperature on the rate at which samples cool through their blocking temperatures whereby non-interacting SD grains would have stronger TRMs when cooled more slowly. York [1978a, 1978b] expanded on the ideas of Stacey and developed a function for blocking temperature dependent on cooling rate. York defined blocking temperature by imagining a time t and temperature T_i at which the field is switched off while the sample continues to cool to ambient temperature. If the magnetization has decayed less than 5%, then T_b

is estimated by T_i. If the sample cools slowly, the magnetization can maintain equilibrium with the applied field to lower temperatures. Because magnetization is a strong (inverse) function of temperature near the Curie Temperature, the net magnetization acquired by slow cooling will be larger than by fast cooling.

Halgedahl et al. [1980] analytically and numerically determined a relationship between cooling rate and the ability of SD magnetite to acquire a TRM. She used the definition for blocking temperature of Néel whereby at T_b, the relaxation time τ is equivalent to the cooling time interval Δt during which τ changes by a factor of e. From this it follows that at the blocking temperature T_b,

$$T_b \frac{\delta_\tau}{\delta T} \cong const,$$

where T_b is the rate of change of T_b, and $\frac{\delta_\tau}{\delta T}$ is the change of τ with temperature. By making the (Néel) assumption of non-interacting uniaxial particles, she derived an analytical expression relating the laboratory magnetization M_L acquired at a cooling rate ($T_{b,L}$ to the magnetization M acquired during a natural cooling rate (T_b) as:

$$\frac{M}{M_L} \cong 1 + ln\left(\frac{T_b}{T_{b,L}}\right)\left(\frac{kT}{2E}\right)$$

where E is the energy barrier between the two easy axes at temperature T and k is Boltzmann's constant. Using the Néel relationship for τ to be $\frac{1}{C}\exp^{\frac{E}{kT}}$ and assuming a value for C, the frequency factor, of 10^{-9} per second and a laboratory value for τ to be 10^2 sec,

Halgedahl estimated $\frac{E}{kT}$ to be $\cong 25$. So, for one order of magnitude difference in cooling rate, M is some 1.05 times M_L. She checked this simple analytical approximation with a more sophisticated numerical approach and found that the analytical approximation performed surprisingly well. The Halgedahl equation therefore predicts a ~5% over estimation of paleointensity for each order of magnitude decrease in cooling rate in nature relative to that used in the laboratory experiment and has been used by, for example, Selkin et al. [2000] to correct intrusive Archean samples for the effect of slow cooling.

Dodson and McClelland-Brown [1980] start from the same Néel assumptions and derived a relationship between magnetization and changes in blocking temperature that result from changes in cooling rate:

$$\frac{\Delta n_b}{n_b} = -\frac{\Delta T_b}{T_b}\left(1 - \frac{T}{M_s}\frac{\delta M_s}{\delta T}\right)$$

where n_b is the magnetization blocked at T_b, Δn_b is that blocked at ΔT_b, M_s is saturation magnetization and $\frac{\delta M_s}{\delta T}$ is the change in saturation with temperature. While not as straightforward as the Halgedahl expression, they calculated that $\frac{\Delta n_b}{n_b}$ would be about 7% larger for each order of magnitude difference in cooling rate.

In the same year, Fox and Aitken [1980] compiled results from unpublished data in PhD theses of N.J. Dunn and J.M.W. Fox and new experiments comparing slowly cooled remanences (cooling times of 2, 2.5 and 16 hours) with those acquired over rapid (cooling times of 3 or 5 minutes). All of their experiments resulted in higher

magnetizations in the slower cooled cases. They reported overestimates of 2-9% for a 2 hour cooling. Assuming that the ratios of cooling times are the same as the ratios between cooling rates at the time of blocking we can compare their results with the predictions of Halgedahl and Dodson and McClelland-Brown. The sense of the cooling rate dependence is the same (slower cooling leads to higher magnetization) and the magnitudes are similar as well (6% and 10% predicted by Halgedahl and Dodson and McClelland-Brown, respectively), 5% for a 2.5 hour cooling (compared to the predicted ∼8% and 10%) and 7-14% for the 16 hour cooling (compared to predictions of 13% and 16%).

McClelland-Brown [1984] repeated the experiments of Fox and Aitken [1980] on synthetic magnetites and titanomagnetites of various sizes and concentrations using cooling times of 2.5 hours and 3 minutes for the slow and fast cooling experiments, respectively. For the non-interacting 'single-domain' (100-180 μm acicular magnetite) she found a 15% over-estimate (compared to predictions of 9% and 12% from Halgedahl [1980] and Dodson and McClelland-Brown [1980], respectively). For the interacting SD experiment, she found that the fast cooled experiment was about 5% greater than the slow cooled one, an opposite effect than that predicted by Néel theory.

Ferk et al. [2010] (see also [Ferk et al., 2014]) analyzed the cooling rate effect for synthetic volcanic glass under a range of laboratory cooling rates (from 0.1 to 15 K/min) and found that the slowest cooled experiments had an 18% larger paleointensity estimate than the laboratory field.

Yu [2011] analyzed synthetic and natural SD samples in cooling rates of 40 K/min and 3 K/min for fast and slow cooling. He found over-estimates of the slow cooling relative to the fast cooling ranging from 3% to 20%.

Berndt et al. [2017] reprised the theoretical development of Néel [1949], York [1978a, 1978b], and Dodson and McClelland-Brown [1980] for non-interacting SD grains. They point out that the treatment of Dodson and McClelland-Brown differed by that of York by a factor of two, owing to differences in the weak field approximation. They also expanded the treatment of rate dependence to heating as well as cooling and developed a novel way of measuring the frequency factor, C, directly. Over the years, this 'constant' has been assumed to be 10^8/s by Stacey and Banerjee [1974] and 10^9/s by Halgedahl [1980]. Moskowitz et al. [1997] also experimentally determined a value of $\sim 10^9$/s. For comparison, the values of Berndt et al. [2017] ranged from 10^{13}/s to $\sim 10^9$/s. While Néel was fully aware that blocking occurs over a range of temperatures, he supposed that the range was quite small and adopted the approximation of a discrete blocking temperature. Berndt et al. [2017] found a range of temperatures of 5-20K over which blocking takes place in practice.

Berndt and Muxworthy [2017] simulated TRM acquisition from Néel theory using a distribution of grain sizes and cooling times ranging from 10 minutes to one million years. Their calculations agreed well with those of Halgedahl et al. [1980], underscoring the possibility of up to 60% overestimates of field strength for slowly cooled rocks.

2.2 Non-Single-Domain Remanances

The situation becomes even more complicated when dealing with grains other than non-interacting SD. First of all, grains that are nominally 'single-domain' behave differently if they interact with neighboring single-domain grains. Scherbakov et al. [1996] showed that in such populations, the dominant energies are not simply those within a single crystal, but instead the so-called 'interaction' energy. How this will affect cooling rate, however, has not been explored.

Stacey [1963] predicted that multi-domain (MD) grains would have the opposite effect of SD grains with MD TRMs being lower when cooled more slowly. He also surmised that so-called 'pseudo-single-domain' (PSD) grains would have an SD-like cooling rate effect, which could be used to distinguish them from MD grains. McClelland-Brown [1984] noted that the 'MD' sample with a grain size range of 2.3 - 65 μm, showed a decreased intensity for the slowly cooled experiment. Yu [2011] also tested PSD (1.06 μm) and MD (18.3 μm) magnetites and natural SD (Tudor Gabbro), PSD (basalts) and MD (granites) studied in previous publications. His natural PSD samples had estimates ranging from 11% underestimation to 18% overestimation, and while the synthetic and natural MD samples were both described as 'nonlinear', his data suggested that the slow cooled experiments had lower TRMs than the fast cooled experiments.

In a comprehensive review of the literature, as well some additional experiments of their own, Biggin et al. [2013] concluded that the cooling rate effect for PSD, MD, or

interacting SD grains is unlikely to exceed 10% (which they deemed 'negligible'). Also, recently, Ferk et al. [2014] showed that small PSD grains had larger TRMs during slow cooling, but the effect was negligible in larger PSD and MD grains.

Absent an analytical theory for PSD and MD grains, Winklhofer et al. [1997] performed 3-D micromagnetic modeling experiments to predict blocking temperatures for a range of magnetite particles. They suggested that fast cooling might result in a particular grain being blocked in an SD state, while during slow cooling, the same grain could be blocked in a vortex state, resulting in a considerable overestimation of the paleofield. Dunlop et al. [1994] and Muxworthy et al. [2013] explain the negative cooling rate effect in MD grains by nucleation of domain walls during cooling. Slower cooling allows more nucleation events, resulting in reduced magnetizations.

In a novel treatment of the cooling rate effect, Muxworthy et al. [2013] used a Preisach based approach developed by Muxworthy et al. [2011] to estimate cooling rate corrections for slowly cooled rocks. Using FORC data, they developed a temperature dependent cooling rate correction that was up to 50% for the Modipe Gabbro whose remanence has a significant contribution of PSD grain sizes.

Two other processes could affect the dependence of magnetization on cooling rate: magnetic disaccommodation [Moskowitz, 1985], and reordering of cations and/or vacancies in the crystal structure [Bowles and Jackson, 2016]. Both of these can occur below the Curie Temperature and would be cooling rate dependent.

There is therefore little consensus of what the cooling rate dependence of TRM should be in even the simplest case of non-interacting SD grains (Halgedahl et al. [1980] versus Dodson and McClelland-Brown [1980]). Furthermore, larger grain sizes should either have a small or even negative effect, yet experimental data for this grain size range are ambiguous. We therefore attempt to address the problem of cooling rate dependence in natural samples with a range of grain sizes. We selected suites of samples based on their behavior during Thellier-Thellier type experiments and subjected them to new experiments using a 'fresh' laboratory acquired thermal remanence in two cooling times ($<$ 1 hour and $\sim$10 hours). We find that proxies for domain state based on hysteresis parameters do not predict cooling rate dependence or accuracy of paleointensity estimates.

Chapter 3

Methods

3.1 Paleointensity Experiment

Studies of paleosecular variation of the geomagnetic field by Lawrence et al. [2009], Sbarbori et al. [2009], Cromwell et al. [2013a, 2013b], and Cromwell et al. [2015] obtained samples from lava flows from Antarctica, Hawaii, Socorro Island, Jan Mayen, and Costa Rica, respectively (see Table 3.1). Samples from these studies were subjected to IZZI experiments [Yu et al., 2004] in the Scripps Institution of Oceanography paleomagnetics laboratory during the original investigations. Based on results from these original experiments (available in the MagIC database), we selected specimens for re-analysis in the present study. The IZZI method is a Königsberger-Thellier-Thellier (see [Tauxe and Yamazaki, 2015] for a recent review) type experiment that replaces the original natural

Table 3.1: Locations, lithologies, age ranges, and citations of samples used in this study.

Locations	Lat. ($^\circ N$)	Long. ($^\circ E$)	Lithology	Age Range	Citation
McMurdo	-76.23	-167.43	basalt	1.26-2.28 Ma	1
Socorro	18.78	-110.98	trachyte	0.35-0.55Ma	2
Hawaii	19.90	-155.58	basalt	1843 CE	3
Jan Mayen	71.03	-8.29	basalt	0.2-0.45 Ma	4
Costa Rica	9.93	-84.09	basalt	< 2 Ma	5

Citations: 1) 10.1029/2008GC002072, 2) 10.1186/BF03352899, 3) 10.1016/j.pepi.2014.12.007, 4) 10.1002/ggge.20174, 5) 10.1002/ggge.20199.

remanence (NRM) with a laboratory thermal remanence (TRM). Data for the *straight* and *curved* sample sets are shown in Figures 3.1 and 3.2, respectively. The experimental protocol alternates steps that cool the specimen from a given temperature in the presence of a laboratory field (infield step, 'I') with cooling in a zero field ('Z' step) at increasing temperatures. The insets in the lower left-hand corners of the first two columns of Figures 3.1 and 3.2 show the progressive demagnetization of the NRM plotted as Zijderveld diagrams [Zijderveld, 1967]. These show univectorial decay to the origin. The data shown in these figures are all in specimen coordinates and have not been corrected to geographic coordinates for the present purpose. The insets in the upper right-hand corners of the first two columns of Figures 3.1 and 3.2 show the progressive demagnetization of the NRM as blue dots and the acquisition of the laboratory TRM as red dots at each temperature step. The order of "infield-zerofield" (IZ) and "zerofield-infield" heating steps (ZI) switches with each subsequent heating step. In-field steps at lower temperatures (pTRM checks) are inserted within every ZI step to test if the capacity to acquire remanence of the specimen

had changed. NRM remaining after each heating step is plotted against the pTRM gained in the so-called 'Arai' plots [Nagata et al., 1963] shown in Figures 3.1 and 3.2.

Many of the original IZZI experiments 'failed' the paleointensity selection criteria adopted by the authors but did not fail pTRM check tests for chemical alteration (see, e.g. Figures 3.1: Column 1 and 3.2: Column 1). The thermal stability of these samples allows us to repeat the IZZI experiments (although on different specimens) including repeated high temperature treatment necessary for testing for a cooling rate dependence.

3.2 Domain State Proxies

As outlined in Chapter 2, there is controversy over the dependence of the cooling rate effect on domain state; hence, we would like to characterize our specimens in terms of domain state. Many methods have been proposed in the literature for doing this, including the classic approach of Day et al. [1977] whereby several ratios of statistics are calculated from hysteresis loops, namely, the ratio of saturation remanence (M_r) to saturation magnetization (M_s) and the ratio of coercivity of remanence (H_{cr}) to coercivity (H_c). More recently, Patterson et al. [2017] proposed a slight modification of these ratios by combining them together into a single 'Bulk Domain Stability' (BDS) statistic. We calculate BDS of Patterson et al. [2017] using the relationship from their Appendix:

$$\text{BDS} = -0.3900\left[\log\left(\frac{B_{cr}}{B_c}\right) - 0.6062\right] + 0.6353\left[\log\left(\frac{M_r}{M_s}\right) + 1.2018\right]$$

Using the values for $\frac{M_r}{M_s}$ and $\frac{B_{cr}}{B_c}$ or 0.5 and 1.5 respectively for the SD/PSD transition of Day et al. [1977], we get a BDS value of 0.74 while values of 4 and 0.05 for the PSD/MD transition translates to a BDS value of 0.57. Note that Dunlop and Ozdemir [1997] point out that the choice of $\frac{B_{cr}}{B_c}$ ratio by Day et al. [1977] of 1.5 is arbitrary and can be between 1 and 2. Using a value of 1 instead yields a BDS of 0.81.

To characterize the samples in terms of hysteresis behavior, we measured hysteresis loops on a sister specimen (< 30 mg) from each sample. These experiments were performed on a Micromag 2900 alternating gradient field magnetometer. Examples of hysteresis loops are shown in Column 3 of Figures 3.1 and 3.2.

Paterson [2011] proposed a different way of assessing domain state by using the curvature of Arai plots. His curvature statistic k is the inverse of the radius of a unit circle that best fits the data in the Arai plot. A straight line on the Arai plot would have a k value of zero and that of a perfect downward bowed circle would be unity. Negative values imply upward bowed Arai plots and values in excess of unity are more highly curved than a circle. Paterson suggested the threshold value of $k < 0.164$ as diagnostic of SD-like behavior and $k > 0.164$ for MD-like behavior. Strictly speaking, k is calculated using all of the data, including points at either end which may be deemed suspect based on failure of a pTRM test, or presence of a small viscous remanence, for example. We therefore used the curvature statistic k' [Paterson et al., 2014] which is the value of k for the measurements actually used in the slope calculation. This combined with a high value for

FRAC (the fraction of remanence used in the slope calculation [Paterson et al., 2014]) protects against using only a small fraction of the data. Here, we calculated the k' statistic for the original experiments using a FRAC of 0.78. Higher values for FRAC were in many cases not possible as the original experiments did not always continue to the maximum blocking temperature. We used the threshold value of 0.164 for k' to separate samples into two broad categories: those with *straight* Arai plots ($k' < 0.164$, Figure 3.1: Column 1) and those with *curved* Arai plots ($k' > 0.164$, Figure 3.3: Column 1). For the present study we chose a total of 24 samples with 12 in each category from the original sample collection with k' values ranging from -0.42 to 1.69.

We prepared specimens from the 24 original samples by cementing small chips ($<$ 1 gm) into a borosilicate glass tube using Whatman filter paper and KaSil glue. These were then thermally demagnetized in a laboratory oven at 580 °C. Following this, the specimens were given a new laboratory controlled total TRM by cooling from 600 °C in a 70 μT field aligned parallel to the specimen $-z$ direction. These 'fresh' TRMs were subjected to an IZZI experiment (see examples in Column 2 of Figure 3.1 and Figure 3.2). After completion of the IZZI experiments on the fresh TRMs, the specimens were given total TRMs as before but cooled at two different rates (calculated using the method of Shaar and Tauxe [2013]): *fast* (43.6 K/min) and *slow* (1.3 K/min). The *fast* cooling step was repeated after the *slow* cooling step to check for alteration. None was detected.

We analyzed our IZZI experimental data with the Thellier GUI program of Shaar and Tauxe [2013] and hysteresis loops with hysteresis magic.py, both in the PmagPy

software package of Tauxe et al. [2016] (https://github.com/PmagPy/PmagPy). For the analysis described here, intensity and curvatures were calculated using all of the data with one exception. For specimen sc02e1-CZB, temperature steps from 0 to 580 °C were used with a FRAC value of 0.96 because this specimen (sc02e1) altered after heating to 580 °C. In this single case, k' was calculated instead of k. Values for k (k') in the fresh experiments ranged from $-.06$ (slightly bowed upward) to 0.329 (significantly curved downward). Intensity estimates ranged from 66.8 to 82.4 μT.

Figure 3.1: Column 1: (a, d, and g) representative Arai plots of *straight* samples from the original experiments. Red (blue) dots are the zerofield-infield (infield-zerofield) steps, and triangles are the pTRM check steps. A threshold value of 0.164 [Paterson, 2011]; [Paterson et al., 2014] for the absolute value of curvature (k'), calculated with a minimum FRAC of 0.78, was used as a threshold to distinguish between straight and curved behavior. Column 2: (b, e, and h) experiments on fresh TRMs. Symbols as in Column 1. k values calculated for the entire data set. Insets in columns 1 and 2 are as follows. Lower left corners: Zijderveld diagrams where components of the magnetization (normalized to NRM) are plotted for each demagnetization step. Blue dots are *X, Y* pairs, and red squares are *X, Z* pairs. Specimens are unoriented. Upper right corners: magnetization versus demagnetization temperature with NRM (blue circles) and pTRM gained (red circles), normalized by the initial NRM. Column 3: (c, f, and i) corresponding hysteresis plots of samples shown in columns 1 and 2. The red curve includes the nonferromagnetic (paramagnetic) contribution, and the blue curve is the resulting curve after subtraction of the paramagnetic slope. TRM = thermal remanent magnetization; NRM = natural remanence magnetization.

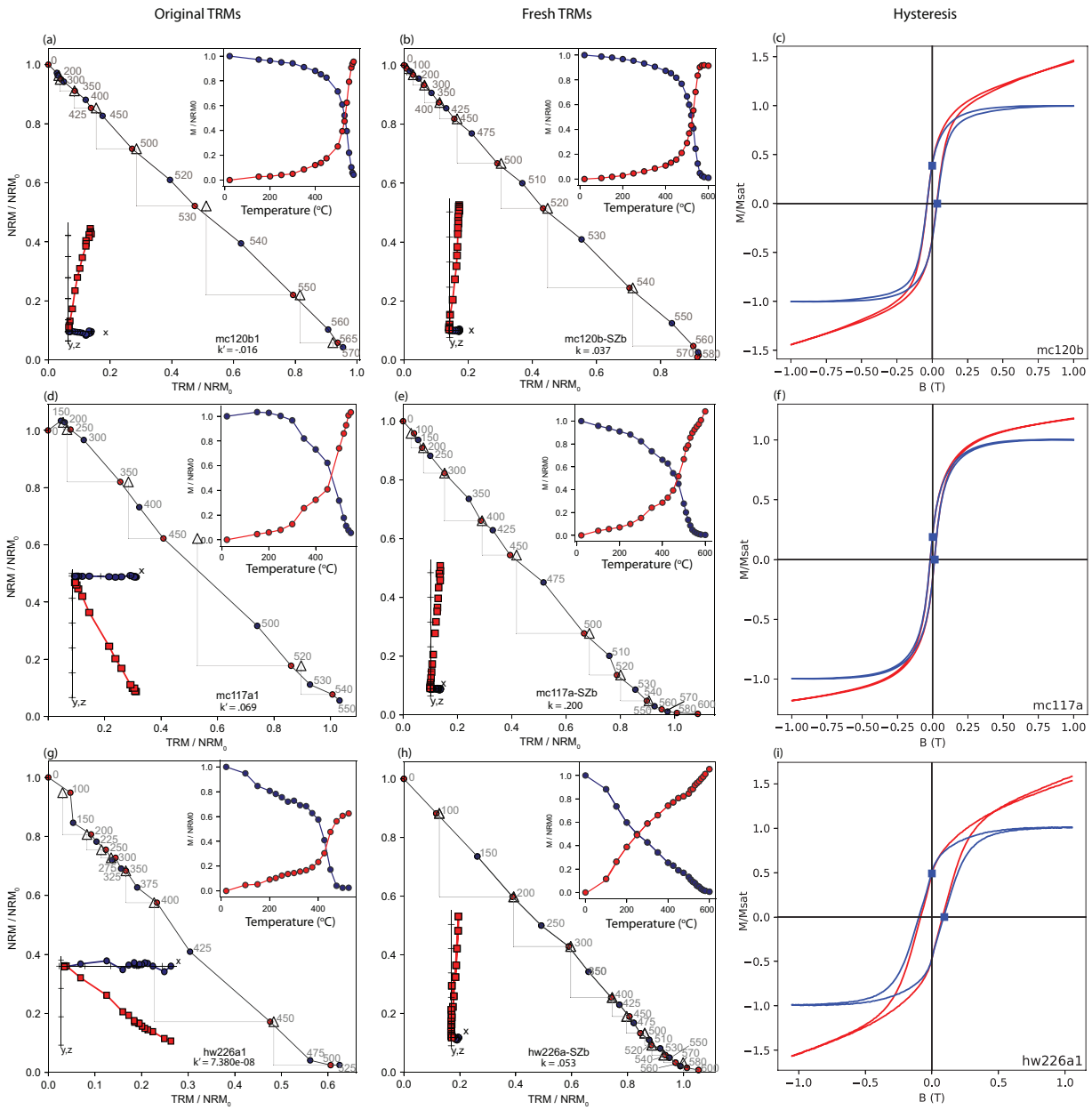
Original TRMs
Fresh TRMs
Hysteresis
(a)
(b)
(c)
(d)
(e)
(f)
(g)
(h)
(i)
NRM / NRM0
TRM / NRM0
M / NRM0
Temperature (°C)
M/Msat
B (T)
mc120b1
k' = -.016
mc120b-SZb
k = .037
mc120b
mc117a1
k' = .069
mc117a-SZb
k = .200
mc117a
hw226a1
k' = 7.380e-08
hw226a-SZb
k = .053
hw226a1

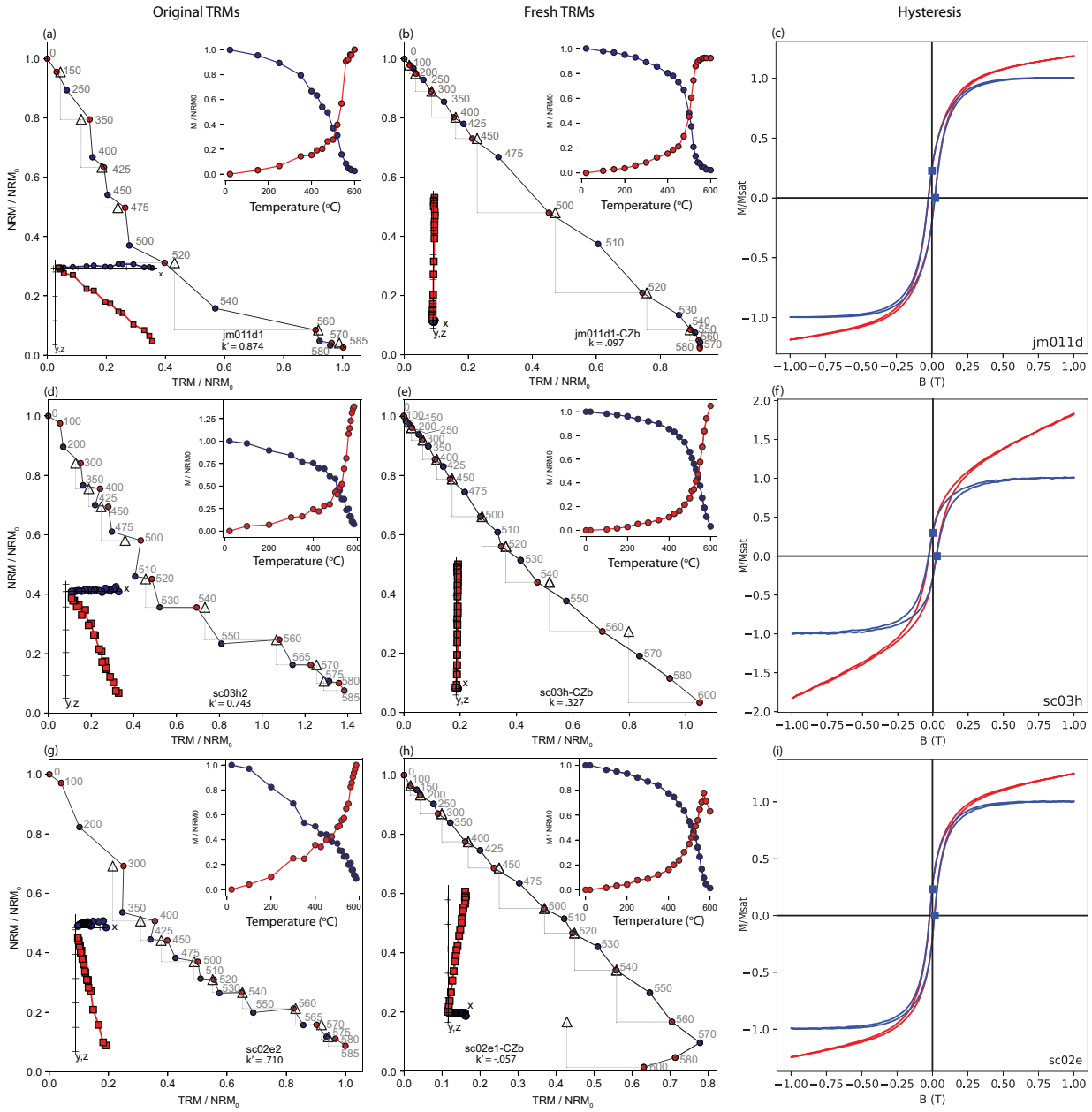

Figure 3.2: Same as Figure 3.1 but for *curved* samples with the exception of Column 2h) which has a k' value calculated excluding the data from the last two temperature steps, as this specimen altered after reheating to 580° C.

Chapter 4

Results

4.1 Domain state proxies

We calculated saturation remanence, M_r, saturation magnetization, M_s, coercivity of remanence, B_{cr} and coercivity, B_c, from the hysteresis loops. We plot the ratios $\frac{M_r}{M_s}$ (squareness) and $\frac{B_{cr}}{B_c}$ in a Day plot [Day et al., 1977] in Figure 4.1a, the squareness versus coercivity [Néel, 1955] in Figure 4.1b and a log-log version of the Day plot in Figure 4.1c, along with the so-called bulk domain stability (BDS) line (in black) of Paterson et al. [2017]. In general, all of the data plot well above the theoretical SD-MD mixing line of Dunlop [2002] and Dunlop and Carter-Stiglitz [2006], underscoring the difficulty in using Day plots to characterize samples in terms of domain state as pointed out by Roberts et al. [2018]. However, although there is considerable overlap on the Day plot, the hysteresis data from the *straight* sample set (squares) have higher squareness values than those from

the *curved* set (circles). Similarly, the data from the *straight* sample set plot above the trend of the *curved* samples in the squareness versus coercivity plot (Figure 4.1b). Higher squareness values indicate that the magnetic remanence of individual magnetic grains is closer to the saturation magnetization, a behavior often used to argue for greater simplicity of domain structures (SD versus MD).

Table 4.1: Data Table for all specimens.

Specimen	Original k′	Fresh k	M_{slow}/M_{fast}	M_r/M_s	BDS	Intensity (μ T)	Marker Color
			Straight				
hw226a-SZb	0.000	0.053	1.065	0.49	0.72	69.3	blue
mc109d-SZb	-0.107	0.042	1.049	0.26	0.46	71.5	blue
mc109e-SZb	-0.087	0.131	1.058	0.27	0.43	71.0	blue
mc111d-SZb	-0.379	-0.037	1.027	0.32	0.57	70.5	blue
mc111e-SZb	-0.423	-0.064	1.037	0.27	0.47	69.8	blue
mc120b-SZb	-0.016	-0.004	1.032	0.39	0.64	74.3	blue
mc120c-SZb	-0.076	-0.003	1.018	0.40	0.67	70.8	blue
mc167d2-SZb	0.000	-0.016	1.082	0.16	0.29	70.8	blue
mc117a-SZb	0.069	0.199	0.969	0.19	0.36	70.0	magenta
mc117b-SZb	0.103	0.209	0.966	0.22	0.39	69.4	magenta
mc117d-SZb	0.115	0.224	0.981	0.20	0.36	70.0	magenta
mc117e-SZb	0.145	0.242	0.999	0.23	0.40	68.2	magenta
			Curved				
cr418f-CZb	0.302	0.258	1.046	0.15	0.27	68.2	orange
cr423c-CZb	1.150	0.258	1.011	0.17	0.31	68.4	orange
sc03f-CZb	0.929	0.194	1.019	0.24	0.44	75.0	orange
sc03h-CZb	0.743	0.329	1.039	0.30	0.53	66.8	orange
sc06d-CZb	1.689	0.210	1.015	0.16	0.25	70.3	orange
cr405g1-CZb	1.370	0.042	1.040	0.12	0.16	69.8	red
jm009c1-CZb	0.873	0.143	1.105	0.19	0.38	68.3	red
jm009d1-CZb	0.694	0.038	1.068	0.20	0.41	73.9	red
jm009f2-CZb	0.923	0.000	1.115	0.21	0.41	67.3	red
jm009i2-CZb	0.607	0.095	1.053	0.20	0.41	80.9	red
jm011d1-CZb	0.874	0.098	1.061	0.23	0.45	71.2	red
sc02e1-CZb*	0.710	-0.057	[0.958]	0.23	0.44	82.4	green

* Value for curvature was k' as opposed to k (see text).

4.2 Paleointensity

Figures 4.2a,b compare the difference in the k' statistic between the original experiments and k calculated for the fresh TRMs for the two groups of samples (*straight* and *curved*). The results fall into five categories.

1. The majority of the *straight* samples retained low k values ($k < 0.164$) in the second heating experiment (blue squares in Figure 4.2a). Four of the 12 specimens (all from the same lava flow mc117) became slightly more curved in the second TRM experiment.
2. The k values of all four mc117 samples were larger in the second experiment (magenta squares in Figure 4.2a) and slightly surpassed the critical $k < 0.164$ value. After the second heating experiment, a slight curvature can be seen on the Arai diagrams (e.g., Figure 3.1e) in the higher temperature heating steps ($>$ 560 °C). It is unknown whether this curvature would have been present in the original experiment because the highest temperature step implemented was 550 °C.
3. All 12 specimens of the originally *curved* samples became "straighter" after the second heating experiment with six of the specimens falling within the $k = \pm$ 0.164 bounds (red circles in Figure 4.2b). This could be the result of disaccommodation or reordering [Moskowitz, 1985; Bowles and Jackson, 2016].

These effects would be much slower in the original cooling than in the laboratory experiment, which would affect the curvature of the Arai plot.

4. Five of the 12 *curved* specimens, while straighter in the fresh experiments, had k values exceeding the 0.164 threshold (orange circles in Figure 4.2b).
5. One notable exception is the negative $k´$ value calculated for sc02e1 (green rimmed, white circle). The original Arai diagram for this sample featured a concave down and "zig-zagged" curve (Figure 3.2d). In the second experiment, the Arai diagram was much straighter until reaching the temperature steps above 570 °C, where a "hook"-like feature is observed, changing the sign of the $k´$ value. We attribute this behavior to alteration of this trachytic specimen, as seen in the pTRM check step at 560 °C (white triangle in Figure 3.2h).

Regardless of the change in curvature from the original to the "fresh TRM" heating experiments, Figures 4.2c,d show that the estimated "paleointensities" calculated from each specimen have a much more significant scatter among the originally *curved* samples compared with the originally *straight* samples (Table 4.1). The *straight* set had interpretations ranging from 68.2 to 74.3 μT with a mean and standard deviation of 70.5 $\pm$ 1.5 μT while the *curved* set ranged from 66.2 to 82.4 μT with a mean of 71.9 $\pm$ 5.2 μT.

Paterson et al. [2017] suggested the use of BDS, a function of $\frac{M_r}{M_s}$ and $\frac{B_{cr}}{B_c}$ as a guide to interpreting paleointensity data. They found a relationship between performance in a

paleointensity experiment and BDS whereby specimens with higher BDS values performed more accurately than those with lower BDS values. In our experiments (Figure 4.3), we find no clear relationship between paleointensity accuracy and BDS.

4.3 Cooling Rate

Figures 4.4 and 4.5 show the results of our cooling rate experiments. In addition to changes in curvature, we found a significant cooling rate dependence for nearly all curvatures (Figure 4.4a,b). The specimens with the highest cooling rate dependence (jm009f2 and jm009c1) had original curvature values significantly higher than the cutoff value of 0.164 recommended by Paterson [2011] (Figure 4.4a). However, the curvature in the fresh TRM experiment was below the cutoff. The cooling rates of cr418f and sc03h, whose curvatures in both the original and fresh TRM experiments were higher than the cutoff, had cooling rates near those predicted for single-domain behavior. Three specimens have negative cooling rates, which many studies have predicted for MD behavior (e.g., [Stacey, 1963; Dunlop et al., 1994; Muxworthy et al., 2003]). These specimens were from lava flow mc117 and had *straight* original curvatures but became slightly more *curved* in the fresh experiments.

We plot the cooling rate dependence from Figure 4.4 against BDS in Figure 4.5. The samples with the highest and lowest cooling rate dependencies all have similar

(moderate) BDS values of around 0.4 with no clear relationship between the two parameters.

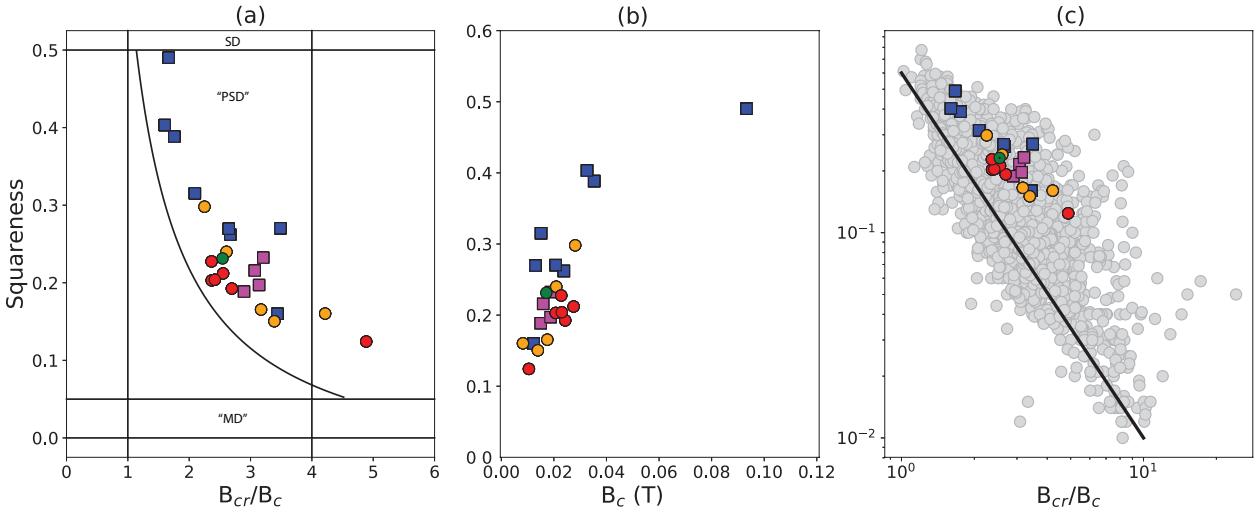

Figure 4.1: a) Day plot [Day et al., 1977] of straight (blue and magenta squares) and curved (red, orange, green circles) specimens. Solid line is SD-MD mixing curve of Dunlop [2002] and Dunlop and Carter-Stiglitz [2006] (see [Tauxe et al., 2010]). b) Plot of squareness (M_r/M_s) against coercivity (B_c). Symbols as in a). c) Log-log plot of data in a) and geological hysteresis data from Paterson et al. [2017] (grey dots). Black line is the 'bulk domain stability' (BDS) trend from Paterson et al. [2017].

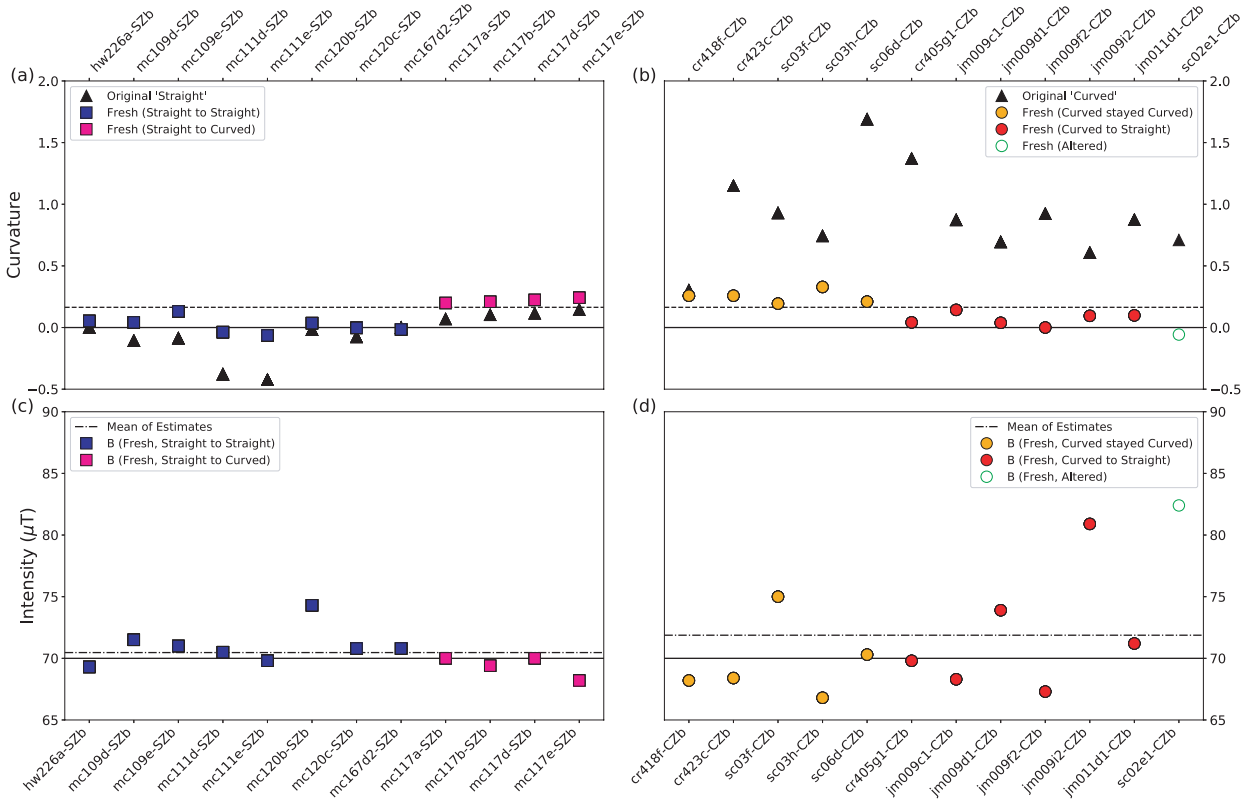

Figure 4.2: a-b) Curvatures (k') from the original experiments (black triangles) versus the k, (k') values those derived from the fresh TRMs (colored squares and circles for *straight* and *curved* experiments, respectively). Dashed line is the 0.164 bound for *straight* ($k' < 0.164$) and *curved* ($k' > 0.164$) Arai plots. Specimen names with '-S' (a,c) were categorized as *straight* and those with '-C' (b,d) were *curved*. c-d) Estimated 'paleointensities' from fresh TRMs acquired in a 70 μT field. Mean values of each group of specimens are shown as dashed-dot lines.

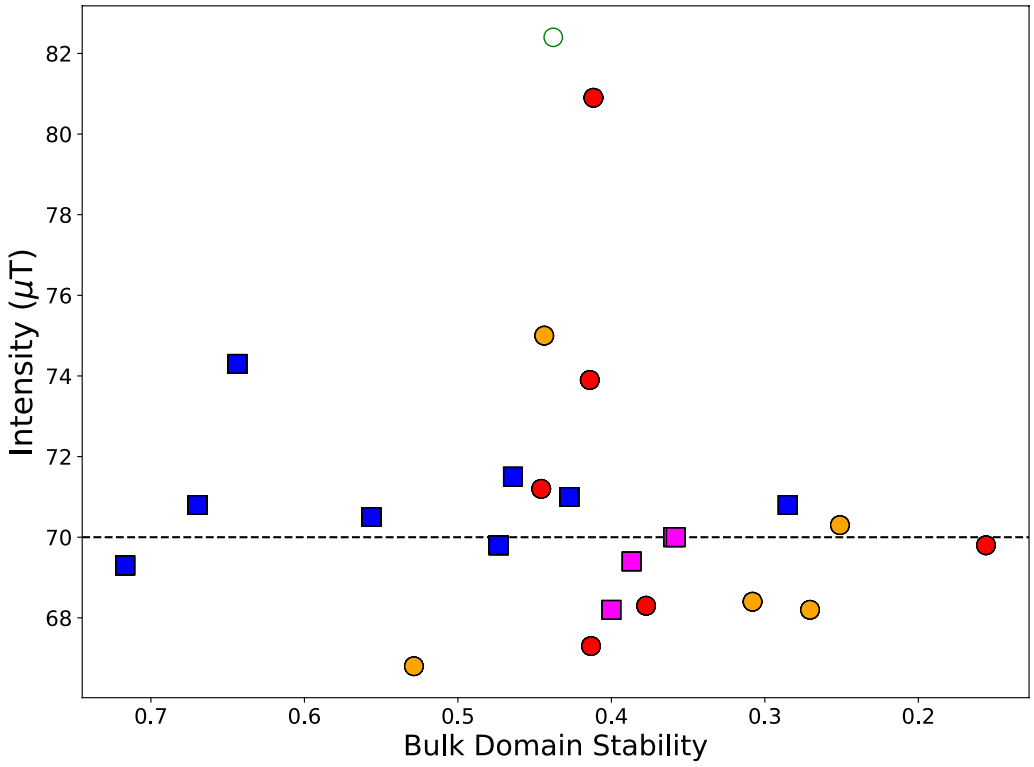

Figure 4.3: Intensity estimate from Figure 4.2 versus sample BDS values (Figure 4.1c), calculated as in Paterson et al. [2017]. Symbols as in Figure 4.2.

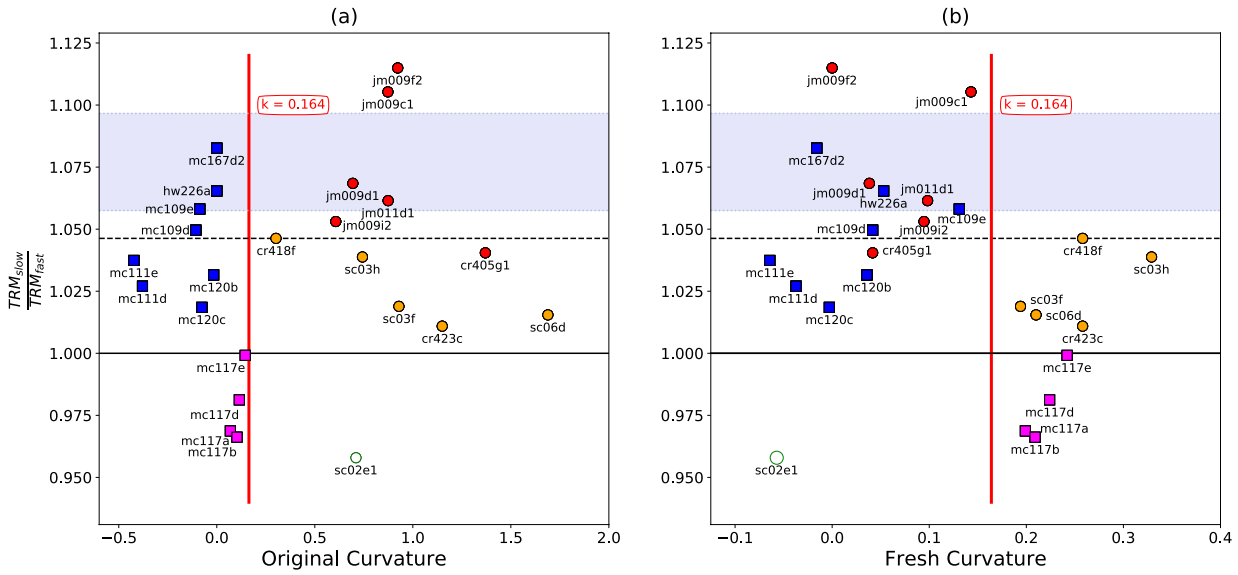

Figure 4.4: Ratio of TRM acquired during slow cooling (1.6 K/min) to fast cooling (43.6 K/min), plotted against curvature (k). The value expected from single domain theory is shown as a dashed line. a) Calculated from the "original" experiments. b) Calculated from the "fresh" experiments. Blue and magenta squares show originally *straight* specimens and red, orange, and hollow green circles show originally *curved* specimens. Each color represents an assigned category based on its observed experimental behavior. The hollow green circle altered during the experiment. The red vertical line is $k = 0.164$, a theoretical critical value separating SD-like from MD-like behavior [Paterson, 2011]. Dashed lines are the mean value of the TRM_{slow}/TRM_{fast} values greater than unity and the lavender boxes are the range predicted from Néel theory [1949] by Halgedahl et al. [1980] and Dodson and McClelland-Brown [1980].

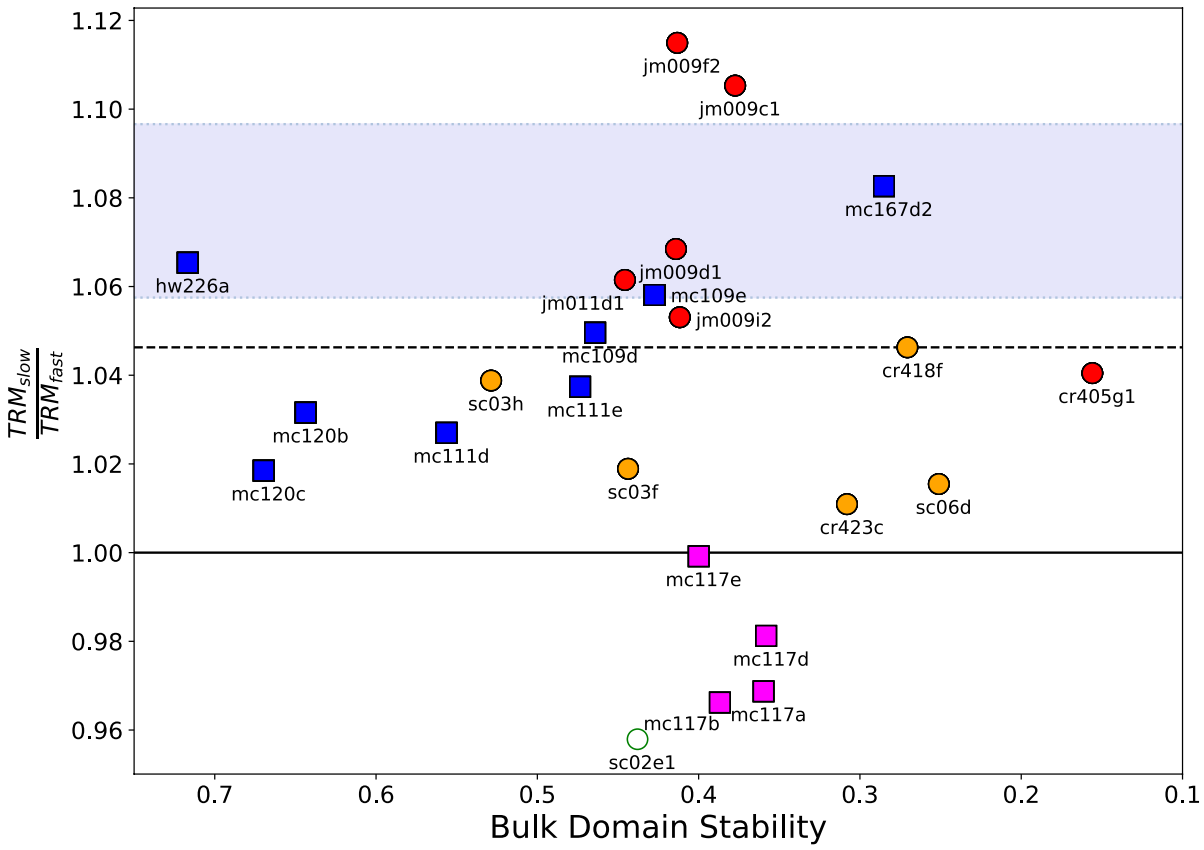

Figure 4.5: Cooling rate ratio plotted against bulk domain stability. Symbols, dashed lines and lavender box same as in Figure 4.4.

Chapter 5

Discussion

As discussed in Chapter 2, there is little consensus in the literature regarding cooling rate dependence versus domain state. We plot empirical cooling rate dependences found in various studies as grey symbols in Figure 5.1 along with the theoretical predictions of Halgedahl et al. [1980] and Dodson and McClelland-Brown [1980] for single-domain grains. In this thesis we examined a variety of natural specimens with a range of parameters generally regarded as proxies for domain state, including curvature of the Arai plots and hysteresis ratios. As described in Chapter 4, we find no consistent pattern of cooling rate dependence versus domain state proxy. We plot the data in Figure 5.1 as colored symbols and ironically, it seems that the largest cooling rate dependence is found in the curved sample set (colored circles) while the straight sample set lower or even a negative cooling rate dependence. It appears that cooling rate cannot be neglected for non-SD material and that the theoretical predictions cannot likely be extrapolated out to

very long cooling rates. We recommend that cooling rate dependence be measured, unless the laboratory and natural cooling rates are similar (as for basaltic glasses [Bowles et al., 2005]).

All of the originally straight samples were specifically chosen because they were rapidly cooled in nature resulting in fine grained, even glassy textures. In the original studies, no cooling rate corrections were applied because the original and laboratory cooling rates are quite similar. Interpretations from the curved samples were not considered reliable in the original studies so no consideration of cooling rate was given. Here we find that although the paleointensity results are certainly more scattered for the curved samples, the average of the 12 estimates was quite accurate. In other words, there does not appear to be a consistent bias and if a sufficient number of specimens are included in the analysis, an accurate result (although less precise) can be estimated. However, cooling rate must be taken into account as it cannot be assumed to be negligible.

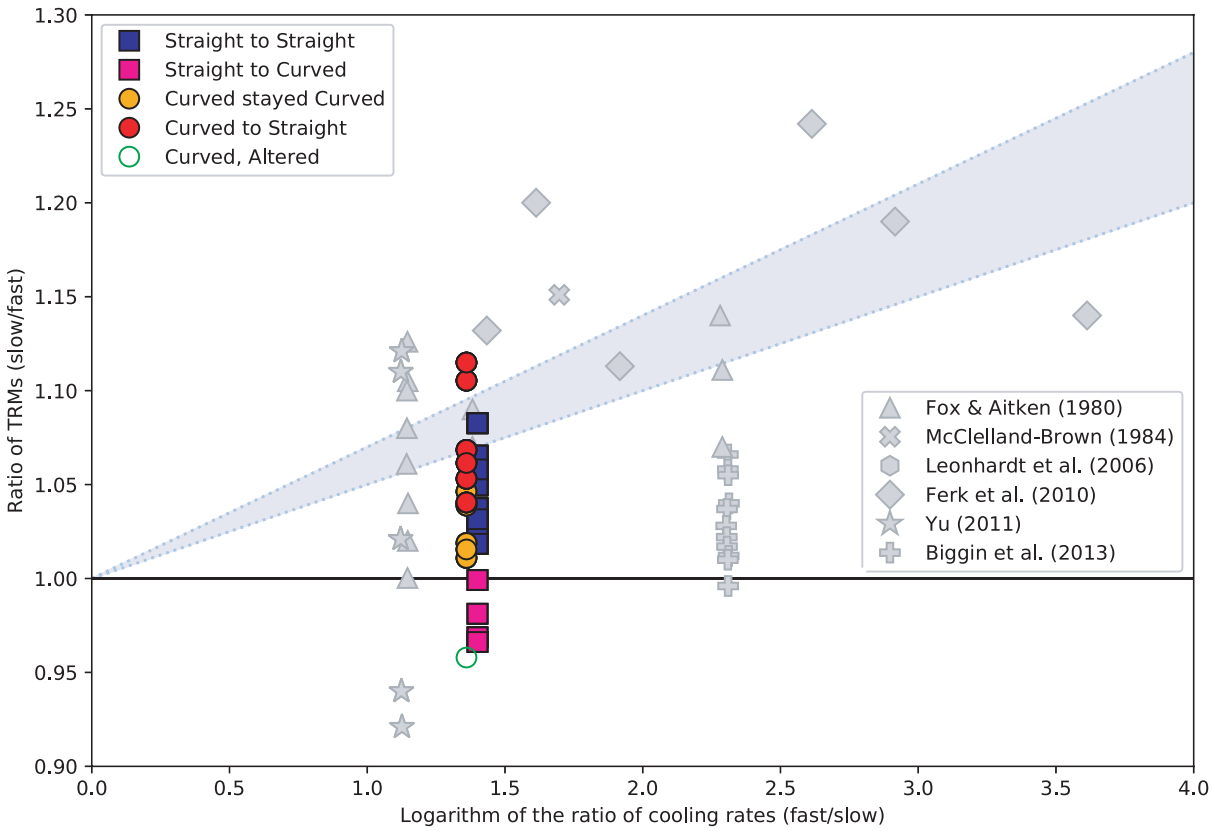

Figure 5.1: The light blue band is the theoretical predictions of Halgedahl et al. [1980] and Dodson and McClelland-Brown [1980], lower and upper bounds of shaded polygon, respectively. Colored circles and squares (offset for clarity) are data from this study; same symbols as previous figures. Gray symbols are a compilation of previously published data, as cited in Chapter 2.

Chapter 6

Conclusions

1. We divided a set of 24 paleomagnetic samples previously analyzed for paleointensity into two groups based on the curvature of their Arai plots. One group had *straight* NRM versus TRM plots frequently considered 'ideal' in paleointensity studies and the other had *curved* plots using the curvature criterion k' of 0.164 that Paterson et al. [2012] recommended as a means to separate 'single-domain' behavior from 'multi-domain.' A total of 12 specimens from each of the *straight* and *curved* sample sets were given a 'fresh' TRM in a laboratory field of 70 μT and the paleointensity experiment was repeated. The fresh TRMs often behaved differently than in the original experiments. All experiments on fresh TRMs of the originally *curved* sample set were much straighter with seven of the 12 having curvatures less than 0.164 threshold

value. Four specimens from the *straight* group, all from the same lava flow, became slightly more curved.

2. Extremely accurate and precise intensities were recovered from the *straight* sample set with a range in estimates from 68.2 to 74.3 μT. The *curved* sample set was much more scattered with results ranging from 66.8 to 82.4 μT. Nonetheless, the average values of the two sets (70.1 and 71.9 μT) were quite close to the laboratory field of 70 μT.
3. A cooling rate dependence of TRM for single-domain remanences is expected from Néel theory [Néel, 1949], whereas larger grain sizes (so-called pseudo-single-domain) are widely thought to have a negligible effect (e.g. [Yu, 2011; Biggin et al., 2013; Ferk et al., 2014]). Apart from the four specimens that were originally straight but became more curved in the fresh TRM experiments (with zero to negative cooling rate dependences), the remaining 20 specimens, regardless of apparent domain state, had a cooling rate dependence of TRM ranging from near zero to ~12%.
4. We performed hysteresis experiments on sister specimens from all samples, calculating the ratios of saturation remanence to saturation and coercivity of remanence to coercivity. From these, we calculated the 'bulk domain stability' index of Paterson et al. [2017] which they claim is a proxy for domain state. BDS estimates and other hysteresis parameters proved to have little predictive value for paleointensity behavior. However, curvature proved to be highly

correlated with both precision of the paleointensity estimates (with higher curvature leading to higher scatter in the results) and to be related to cooling rate dependence (with higher curvature associated with lower cooling rate (or even negative cooling rate) dependence.

The abstract and chapter sections of this thesis, in full, are modified versions of a publication as it appears in Geochemistry, Geophysics, Geosystems: Santos, C. N., & Tauxe, L. (2019). Investigating the accuracy, precision, and cooling rate dependence of laboratory-acquired thermal remanences during paleointensity experiments. *Geochem., Geophys., Geosys.*, *20*, 383–397. doi.org/10.1029/2018GC007946. The thesis author is the primary investigator and author of this paper.

value. Four specimens from the *straight* group, all from the same lava flow, became slightly more curved.

2. Extremely accurate and precise intensities were recovered from the *straight* sample set with a range in estimates from 68.2 to 74.3 μT. The *curved* sample set was much more scattered with results ranging from 66.8 to 82.4 μT. Nonetheless, the average values of the two sets (70.1 and 71.9 μT) were quite close to the laboratory field of 70 μT.

3. A cooling rate dependence of TRM for single-domain remanences is expected from Néel theory [Néel, 1949], whereas larger grain sizes (so-called pseudo-single-domain) are widely thought to have a negligible effect (e.g. [Yu, 2011; Biggin et al., 2013; Ferk et al., 2014]). Apart from the four specimens that were originally straight but became more curved in the fresh TRM experiments (with zero to negative cooling rate dependences), the remaining 20 specimens, regardless of apparent domain state, had a cooling rate dependence of TRM ranging from near zero to ~12%.

4. We performed hysteresis experiments on sister specimens from all samples, calculating the ratios of saturation remanence to saturation and coercivity of remanence to coercivity. From these, we calculated the 'bulk domain stability' index of Paterson et al. [2017] which they claim is a proxy for domain state. BDS estimates and other hysteresis parameters proved to have little predictive value for paleointensity behavior. However, curvature proved to be highly

correlated with both precision of the paleointensity estimates (with higher curvature leading to higher scatter in the results) and to be related to cooling rate dependence (with higher curvature associated with lower cooling rate (or even negative cooling rate) dependence.

The abstract and chapter sections of this thesis, in full, are modified versions of a publication as it appears in Geochemistry, Geophysics, Geosystems: Santos, C. N., & Tauxe, L. (2019). Investigating the accuracy, precision, and cooling rate dependence of laboratory-acquired thermal remanences during paleointensity experiments. *Geochem., Geophys., Geosys.*, *20*, 383–397. doi.org/10.1029/2018GC007946. The thesis author is the primary investigator and author of this paper.

References

[Ben-Yosef et al., 2010] Ben-Yosef, E., Tauxe, L., and Levy, T. (2010). Archaeomagnetic dating of copper smelting site f2 in the timna valley (israel) and its implications for the modelling of ancient technological developments. *Archaeometry*, 52:110–1121.

[Berndt and Muxworthy, 2017] Berndt, T. and Muxworthy, A. (2017). Paleomagnetic field reconstruction from mixtures of titanomagnetites. *Earth Planet. Sci. Letters*, 465:70–81.

[Berndt et al., 2017] Berndt, T., Paterson, G., Cao, C., and Muxworthy, A. (2017). Experimental test of the heating and cooling rate effect on blocking temperatures. *Geophys. J. Int.*, 210:255–269.

[Biggin et al., 2013] Biggin, A., Badejo, S., Hodgson, E., Muxworthy, A., Shaw, J., and Dekkers, M. (2013). The effect of cooling rate on the intensity of thermoremanent magnetization (trm) acquired by assemblages of pseudo-single domain, multidomain and interacting single-domain grains. *Geophys. J. Int.*, 193:1239–1249.

[Biggin et al., 2012] Biggin, A., Steinberger, B., Aubert, J., Suttie, N., Holme, R., Torsvik, T. H., van der Meer, D., and van Hinsbergen, D. (2012). Possible links between long-term geomagnetic variations and whole-mantle convection processes. *Nature Geoscience*, 5:526–533.

[Bowles et al., 2005] Bowles, J., Gee, J. S., Kent, D., Bergmanis, E., and Sinton, J. (2005). Cooling rate effects on paleointensity estimates in submarine basaltic glass nad implications for dating young flows. *Geochem. Geophys. Geosys.*, 6:Q07002, doi:10.1029/2004GC000900.

[Bowles and Jackson, 2016] Bowles, J. and Jackson, M. (2016). Effects of titanomagnetite reordering processes on thermal demagneitzaiton and paleointensity experiments. *Geochem. Geophys. Geosys.*, 17.

[Cromwell et al., 2013a] Cromwell, G., Constable, C., Staudigel, H., Tauxe, L., and Gans, P. (2013a). Revised and updated paleomagnetic results from costa rica. *Geochem. Geophys. Geosys.*, 14.

[Cromwell et al., 2013b] Cromwell, G., Tauxe, L., Staudigel, H., Constable, C., Koppers, A., and Pedersen, R.-B. (2013b). Evidence for long-term hemispheric asymmetry in the geomagneitc field: results from high northern latitudes. *Geochem. Geophys. Geosys.*, 14.

[Cromwell et al., 2015] Cromwell, G., Tauxe, L., Staudigel, H., and Ron, H. (2015). Paleointensity estimates from historic and modern hawaiian lava flows using basaltic volcanic glass as a primary source material. *Phys. Earth Planet. Int.*, 241:44–56.

[Day et al., 1977] Day, R., Fuller, M. D., and Schmidt, V. A. (1977). Hysteresis properties of titanomagnetites: grain size and composition dependence. *Phys. Earth Planet. Inter.*, 13:260–266.

[Dodson and McClelland-Brown, 1980] Dodson, M. and McClelland-Brown, E. (1980). Magnetic blocking temperatures of single-domain grains during slow cooling. *J. Geophys. Res.*, 85:2625–2637.

[Dunlop et al., 1994] Dunlop, D., Newell, A., and Enkin, R. J. (1994). Transdomain thermoremanent magnetization. *Journal of Geophysical Research*, 99:19,741–19,755.

[Dunlop and Ozdemir, 1997] Dunlop, D. and Ozdemir, O. (1997). *Rock Magnetism: Fundamentals and Frontiers*. Cambridge Studies in Magnetism. Cambridge University Press.

[Dunlop, 2002] Dunlop, D. J. (2002). Theory and application of the day plot (mrs/ms versus hcr/hc) 1. theoretical curves and tests using titanomagnetite data. *J. Geophys. Res.*, 107:doi:10.1029/2001JB000486.

[Dunlop, 2011] Dunlop, D. J. (2011). Physical basis of the thellier-thellier and related paleointensity methods. *Phys. Earth and Planet. Inter.*, 187:118–138.

[Dunlop and Carter-Stiglitz, 2006] Dunlop, D. J. and Carter-Stiglitz, B. (2006). Day plots of mixtures of superparamagnetic, single-domain, pseudosingle-domain, and multidomain magnetites. *J. Geophy. Res.*, 111.

[Ferk et al., 2010] Ferk, A., Aulock, F. v., Leonhardt, R., Hess, K.-U., and Dingwell, D. (2010). A cooling rate bias in paleointensity determination from volcanic glass: An experimental demonstration. *J. Geophys. Res.*, 115:8pp.

[Ferk et al., 2014] Ferk, A., Leonhardt, R., Hess, K. U., Koch, S., Egli, R., Krasa, D., and Dingwell, D. (2014). Influence of cooling rate onthe thermoremanence of magnetite grains: Identifying the role of different magnetic domain states. *J. Geophys. Res.*, 119:1599–1606.

[Fox and Aitken, 1980] Fox, J. M. W. and Aitken, M. J. (1980). Cooling-rate dependence of thermoremanent magnetization. *Nature*, 283:462–463.

[Halgedahl et al., 1980] Halgedahl, S., Day, R., and Fuller, M. (1980). The effect of cooling rate on the intensity of weak-field trm in single-domain magnetite. *J. Geophys. Res*, 85:3690–3698.

[Lawrence et al., 2009] Lawrence, K. P., Tauxe, L., Staudigel, H., Constable, C., Koppers, A., McIntosh, W. C., and Johnson, C. L. (2009). Paleomagnetic field properties near the southern hemisphere tangent cylinder. *Geochem. Geophys. Geosyst.*, 10, Q01005.

[McClelland-Brown, 1984] McClelland-Brown, E. (1984). Experiments on TRM intensity dependence on cooling rate. *Geophysical Research Letters*, 11:205–208.

[Moskowitz et al., 1997] Moskowitz, B., Frankel, R., Walton, S., Dickson, D., Wong, K., Douglas, T., and Mann, S. (1997). Determination of the preexponential frequency factor for superparamagnetic maghemite particles in magnetoferritin. *J. Geophys. Res.*, 102:22,671–22,680.

[Moskowitz, 1985] Moskowitz, B. M. (1985). Magnetic viscosity, diffusion affer effect and disacomodation in natural and synthetic samples. *Geophys. J. R. astr. Soc.*, 82:143–161.

[Muxworthy et al., 2003] Muxworthy, A., Dunlop, D., and Williams, W. (2003). High-temperature magnetic stability of small magnetite particles. *J. Geophy. Res.*, 108:2281.

[Muxworthy et al., 2013] Muxworthy, A., Evans, M., Scourfield, S., and King, J. (2013). Paleointensity results from the late-archaen modipe gabbro of botswana. *Geochem. Geophys. Geosys.*, 14.

[Muxworthy et al., 2011] Muxworthy, A. R., Heslop, D., and Paterson, G.and Michalk, D. (2011). A preisach method for estimating absolute paleofield intensity under the constraint of using only isothermal measurements: 2) experimental testing. *J. Geophys. Res.*, 116:B04103, doi:10.1029/2010JB007844.

[Nagata et al., 1963] Nagata, T., Arai, Y., and Momose, K. (1963). Secular variation of the geomagnetic total force during the last 5000 years. *J. Geophys. Res.*, 68:5277–5282.

[Néel, 1949] Néel, L. (1949). Théorie du trainage magnétique des ferromagnétiques en grains fines avec applications aux terres cuites. *Ann. Geophys.*, 5:99–136.

[Néel, 1955] Néel, L. (1955). Some theoretical aspects of rock-magnetism. *Adv. Phys*, 4:191–243.

[Paterson et al., 2012] Paterson, G., Biggin, A., Yamamoto, Y., and Pan, Y. X. (2012). Towards the robust selection of thellier-type paleointensity data: The influence of experimental noise. *Geochem. Geophys. Geosys.*, 13:Q05Z43, doi:10.1029/2012GC004046.

[Paterson et al., 2017] Paterson, G., Muxworthy, A., Yamamoto, Y., and Pan, Y. (2017). Bulk magnetic domain stability controls paleointensity fidelity. *Proc. Nati. Acad.of Sci.*, 114:13120–13125.

[Paterson et al., 2014] Paterson, G., Tauxe, L., Biggin, A., Shaar, R., and Jonestrask, L. (2014). On improving the selection of thellier-type paleointensity data. *Geochem. Geophys. Geosys.*, 15:1–13.

[Paterson, 2011] Paterson, G. A. (2011). A simple test for the presence of multidomain behavior during paleointensity experiments. *J. Geophys. Res.*, 116(B10104).

[Roberts et al., 2018] Roberts, A., Tauxe, L., Heslop, D., Zhao, X., and Jiang, Z. (2018). A critical appraisal of the 'day' diagram. *J. Geophys. Res.*, 123:2618–2644.

[Sbarbori et al., 2009] Sbarbori, E., Tauxe, L., Gogichaishvili, A., Urrutia-Fucugauchi, J., and Bohrson, W. (2009). Paleomagnetic behavior of volcanic rocks from isla socorro, mexico. *Earth Planets and Space*, 61:191–204.

[Selkin et al., 2000] Selkin, P., Gee, J., Tauxe, L., Meurer, W., and Newell, A. (2000). The effect of remanence anisotropy on paleointensity estimates: A case study from the archean stillwater complex. *Earth Planet. Sci. Lett.*, 182:403–416.

[Shaar and Tauxe, 2013] Shaar, R. and Tauxe, L. (2013). Thellier_gui: An integrated tool for analyzing paleointensity data from thellier-type experiments. *Geochem. Geophys. Geosys.*, 14:677–692.

[Shcherbakov et al., 1996] Shcherbakov, V. P., Sycheva, N., and Lamash, B. E. (1996). Monte carlo modelling of trm and crm acquisition and comparison of their properties in an ensemble of interacting sd grains. *Geophy. Res. Lett.*, 23:2827–2830.

[Stacey, 1963] Stacey, F. D. (1963). The physical theory of rock magnetism. *Adv. Phys.*, 12:45–133.

[Stacey and Banerjee, 1974] Stacey, F. D. and Banerjee, S. K. (1974). *The Physical Principles of Rock Magnetism*, volume 5 of *Developments in Solid Earth Geophysics*. Elsevier Sci. Publ. Co.

[Tauxe et al., 2010] Tauxe, L., Banerjee, S. K., Butler, R., and van der Voo, R. (2010). *Essentials of Paleomagnetism*. University of California Press, Berkeley.

[Tauxe et al., 2016] Tauxe, L., Shaar, R., Jonestrask, L., Swanson-Hysell, N., Minnett, R., Koppers, A. A. P., Constable, C. G., Jarboe, N., Gaastra, K., and Fairchild, L. (2016). Pmagpy: Software package for paleomagnetic data analysis and a bridge to the magnetics information consortium (magic) database. *Geochem. Geophys. Geosys.*, 17.

[Tauxe and Yamazaki, 2015] Tauxe, L. and Yamazaki, T. (2015). Paleointensities. In Kono, M., editor, *Geomagnetism*, volume 5 of *Treatise on Geophysics*, pages 461–509. Elsevier, 2nd edition edition.

[Thellier, 1938] Thellier, E. (1938). Sur l'aimantation des terres cuites et ses applications géophysique. *Ann. Inst. Phys. Globe Univ. Paris*, 16:157–302.

[Thellier and Thellier, 1959] Thellier, E. and Thellier, O. (1959). Sur l'intensité du champ magnétique terrestre dans le passé historique et géologique. *Ann. Geophys.*, 15:285–378.

[Wernsdorfer et al., 1997] Wernsdorfer, W., Orozco, E. B., Hasselbach, K., Benoit, A., Barbara, B., Demoncy, N., Loiseau, A., Pascard, H., and Mailly, D. (1997). Experimental evidence of the néel-brown model of magnetiza- tion reversal. *Phys. Rev. Lett.*, 78:1791–1794.

[Winklhofer et al., 1997] Winklhofer, M., Fabian, K., and Heider, F. (1997). Magnetic blocking temperatures of magnetite calculated with a three-dimensional micromagnetic model. *J. Geophys. Res.*, 102:22,695–22,709.

[York, 1978a] York, D. (1978a). A formula describing both magnetic iand isotopic blocking temperatures. *Earth and Planet. Sci. Lett.*, 39:89–93.

[York, 1978b] York, D. (1978b). Magnetic blocking temperature. *Earth and Planet. Sci. Lett.*, 39:94–97.

[Yu, 2011] Yu, Y. (2011). Importance of cooling rate dependence of thermoremanence in paleointensity determination. *J. Geophys. Res.*, 116.

[Yu et al., 2004] Yu, Y., Tauxe, L., and Genevey, A. (2004). Toward an optimal geomagnetic field intensity determination technique. *Geochemistry, Geophysics, Geosystems*, 5(2):Q02H07, doi:10.1029/2003GC000630.

[Zijderveld, 1967] Zijderveld, J. D. A. (1967). *A.C. demagnetization of rocks: Analysis of results*. Methods in Paleomagnetism. Chapman and Hall.